



**Manchester  
Metropolitan  
University**

---

Parikh, V and Kadiwala, J and Hidalgo, A and Holt, C and Sunami, M and Mirraftab, M and Shakur, R and Azzawi, M (2018) Small diameter helical vascular scaffolds support endothelial cell survival. *Nanomedicine: Nanotechnology, Biology and Medicine*, 14 (8). ISSN 1549-9634

---

**Downloaded from:** <http://e-space.mmu.ac.uk/621429/>

**Version:** Accepted Version

**Publisher:** Elsevier

**DOI:** <https://doi.org/10.1016/j.nano.2018.08.005>

**Usage rights:** Creative Commons: Attribution-Noncommercial-No Derivative Works 4.0

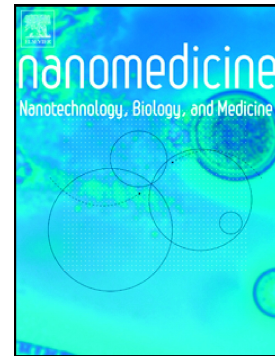
Please cite the published version

<https://e-space.mmu.ac.uk>

## Accepted Manuscript

Small diameter helical vascular scaffolds support endothelial cell survival

Vijay Parikh, Juned Kadiwala, Araida Hidalgo Bastida, Cathy Holt, Mohammad Sanami, Mohsen Miraftab, Rameen Shakur, May Azzawi



PII: S1549-9634(18)30509-4  
DOI: doi:[10.1016/j.nano.2018.08.005](https://doi.org/10.1016/j.nano.2018.08.005)  
Reference: NANO 1856

To appear in: *Nanomedicine: Nanotechnology, Biology, and Medicine*

Received date: 29 March 2018  
Revised date: 12 July 2018  
Accepted date: 10 August 2018

Please cite this article as: Vijay Parikh, Juned Kadiwala, Araida Hidalgo Bastida, Cathy Holt, Mohammad Sanami, Mohsen Miraftab, Rameen Shakur, May Azzawi , Small diameter helical vascular scaffolds support endothelial cell survival. *Nano* (2018), doi:[10.1016/j.nano.2018.08.005](https://doi.org/10.1016/j.nano.2018.08.005)

This is a PDF file of an unedited manuscript that has been accepted for publication. As a service to our customers we are providing this early version of the manuscript. The manuscript will undergo copyediting, typesetting, and review of the resulting proof before it is published in its final form. Please note that during the production process errors may be discovered which could affect the content, and all legal disclaimers that apply to the journal pertain.

**REVISED VERSION**

**Title:** 'Small diameter helical vascular scaffolds support endothelial cell survival'.

**Authors:** *Vijay Parikh,<sup>a,b</sup> Juned Kadiwala,<sup>c</sup> Araida Hidalgo Bastida,<sup>a</sup> Cathy Holt,<sup>d</sup> Mohammad Sanami,<sup>b</sup> Mohsen MirafTAB,<sup>b,e</sup> Rameen Shakur,<sup>c\*</sup> May Azzawi<sup>a\*</sup>*

<sup>a</sup> Cardiovascular Research Group, School of Healthcare Science, Manchester Metropolitan University, Manchester, M1 5GD , United Kingdom

<sup>b</sup> Institute for Materials Research and Innovation (IMRI), University of Bolton, Manchester, BL3 5AB, United Kingdom

<sup>c</sup> Wellcome Trust Sanger Institute, Wellcome Trust Genome Campus, University of Cambridge, Cambridge, UK

<sup>d</sup> Institute for Cardiovascular Science, University of Manchester , Manchester, UK.

<sup>e</sup> Medical Device Consultants Limited, Wilmslow, SK9 4JJ, U.K.

**\* Address for correspondence:** Dr May Azzawi, Cardiovascular Research Group, School of Healthcare Science, Manchester Metropolitan University, Manchester, M1 5GD, United Kingdom. Telephone +44(0) 161 247 3332. Email m.azzawi@mmu.ac.uk; Dr Rameen Shakur, Wellcome Trust Sanger Institute, Wellcome Trust Genome Campus, University of Cambridge, Cambridge, UK. Email rs16@sanger.ac.uk

Word count for abstract: 150

Word count for manuscript: 4,998

Number of references: 47

Number of figures: 4

Number of tables: 2

Number of Supplementary online-only files, if any: 1

**Conflict of interest:** The scaffold design is detailed in a filed patent (Patent Application No: GB1616064).

**Funding:** This work was supported by a 'Joint health accelerator grant' from the University of Manchester and Manchester Metropolitan University (2015/16).

**Abstract** (=150 words)

There is an acute clinical need for small-diameter vascular grafts as a treatment option for cardiovascular disease. Here, we used an intelligent design system to recreate the natural structure and hemodynamics of small arteries. Nano-fibrous tubular scaffolds were fabricated from blends of polyvinyl alcohol and gelatin with inner helices to allow a near physiological spiral flow profile, using the electrospinning technique. Human coronary artery endothelial cells (ECs) were seeded on the inner surface and their viability, distribution, gene expression of mechanosensitive and adhesion molecules compared to that in conventional scaffolds, under static and flow conditions. We show significant improvement in cell distribution in helical vs conventional scaffolds ( $94\% \pm 9\%$  vs  $82\% \pm 7.2\%$ ;  $p < 0.05$ ) with improved responsiveness to shear stress and better ability to withhold physiological pressures. Our helical vascular scaffold provides an improved niche for EC growth and may be attractive as a potential small diameter vascular graft.

**Keywords**

Scaffold; helical; vascular; endothelial; shear stress

## Background

Cardiovascular disease (CVD) is a leading cause of death worldwide <sup>1</sup>. In particular, coronary artery disease (CAD) affecting small and medium-sized blood vessels accounts for 53% of the total mortality <sup>1, 2</sup>. Despite significant improvement in treatment options, the therapeutic gold standard remains the coronary artery bypass graft (CABG) <sup>3</sup>. The most preferable option for these transplants are autologous grafts but many patients lack suitable vessels for grafting due to pre-existing vascular disease, amputation, or previous harvest <sup>3, 4, 5</sup>. Even in the case of synthetic grafts, which have been used as an alternative for large diameter vascular grafts with considerable success rates, they have not proved to be very effective for smaller diameter vessels <sup>5</sup>.

Two major causes for early small diameter graft failure are hemodynamic mismatch between the host artery and the graft; and the lack of graft endothelisation <sup>6, 7</sup>. A healthy, confluent inner endothelium is essential in maintaining vascular homeostasis through the release of mediators that modulate vessel diameter, including nitric oxide <sup>8</sup>. An intact endothelial layer also acts as a continuous, structural and thrombo-resistant barrier between circulating blood and the wall of the vascular graft <sup>9</sup>. Therefore, enabling the seeding and growth of a physiologically healthy endothelium on the inner wall of the implanted vascular graft is a pre requisite for its survival. The hemodynamic environment within the vascular graft also plays a major role for its survival after implantation <sup>10</sup>. In small diameter vessels, hemodynamics is mainly represented in terms of impedance to flow, wall

shear stress (WSS), velocity profile of blood, and flow separation. For larger diameter vessels, the effect of impedance is largely suppressed by higher blood flow rate, which help to absorb greater energy of the disturbance compared to smaller diameter counterparts. Such disturbed flow behaviour of blood is implicated in the formation of atherosclerotic plaques and phenomena such as thrombogenesis, arterogenesis, endothelial cell (EC) damage, intimal thickening and hyperplasia<sup>11</sup>.

The geometry of arteries influences their blood flow motion and hence their biology and susceptibility to disease. It is recognized that the geometry of natural blood vessels is far more complicated than that of model vessels, which influences the local flow pattern and its velocity distribution<sup>12, 13</sup>. Native arterial geometry is three-dimensional, causing blood to flow in a spiral/ helical manner<sup>14, 15</sup>. In a survey of a 3 dimensional arterial flow pattern in a group of 42 volunteers, eleven arterial sites were examined, including the common carotid artery and femoral arteries, spiral laminar flow was shown as the predominant flow pattern<sup>16</sup>. Spiral laminar flow has been shown to provide relatively uniform WSS and inhibit flow stagnation favouring EC growth and release of arteroprotective mediators that improve patency<sup>17, 18, 19</sup>. Therefore, improvement in blood flow haemodynamics in terms of spiral/helical blood flow is essential to enhance the success rate of small diameter vascular grafts in the long term.

Exposure of ECs to unidirectional laminar shear stress (imparted by the frictional drag of flowing blood within the arteries) is associated with upregulation of mechanosensor molecules. These trigger the signalling of mechanotransduction pathways and induction of a number of mechanosensitive transcription factors, such as Piezo 1 and Nuclear factor-like 2 (Nrf-2) which is a master antioxidant regulator and also associated with arteroprotective

responses<sup>19</sup>. These signal transduction mechanisms stimulate the release of vasoactive molecules, such as nitric oxide and prostacyclin that modulate arterial diameter<sup>9</sup>. In contrast, exposure of coronary arteries to asynchronous disturbed flow has been demonstrated to elicit a pathologic gene expression pattern<sup>20, 21</sup>. For long-term graft success it is thus necessary that the hemodynamics generated maintain the expression of mechanosensitive genes and support an atheroprotective phenotype.

A further cause for small diameter graft failure is the surface mismatch, which hinders graft endothelialisation after implantation<sup>22,23</sup>. Blood vessels are well-organized hierarchical fibrous structures with an extracellular matrix (ECM) that realigns at the nanometre scale. Electrospinning technology enables the fabrication of nano-structured vascular scaffolds with a complex porous architecture. Using appropriate polymers of synthetic or natural origin, these constructs can replicate the biomechanical and structural properties of native vessel walls providing support for cell attachment, proliferation and differentiation<sup>24, 25, 26</sup>. Moreover, the mechanical and biological properties of fibers can easily be tuned by varying material composition, not easily achievable using other nano-scaffold fabrication methods<sup>25</sup>. Hence, in addition to matching the natural vessel's nano and macro structure, including wall thickness, this fabrication method should also replicate other important biomechanical indices, such as burst pressure, elasticity and compliance, which are key to graft function<sup>25, 27</sup>. Synthetic polymer materials are often employed in vascular graft designs mainly due to flexibility in tailoring their mechanical properties. Of particular interest, is poly [Vinyl Alcohol] (PVA) since it is water soluble, biocompatible, biodegradable and has excellent chemical and thermal stability.<sup>28</sup> Furthermore, hydrogels made from PVA exhibit tissue-like elasticity and mechanical strength, with microscopic properties similar to those of native

arterial tissue.<sup>29, 30</sup> PVA can be co-spun with natural molecules, such as collagen, which constitutes the major architecture of the native ECM, in order to provide cell attachment sites for improved cell seeding. As gelatin is prepared by partial hydrolysis of collagen it has high biocompatibility and bioactivity. Furthermore, gelatin can react with hydroxyl groups and positively charged polymers such as PVA to create a 3 dimensional porous architecture, providing a good substrate for the adhesion and proliferation of vascular endothelial cells.<sup>31</sup>  
<sup>32</sup> Hence, PVA-gelatin blends show promise for vascular graft applications.<sup>32</sup>

The objective of the present study is to fabricate a small diameter vascular scaffold that closely mimics the ultrastructure and haemodynamics of native vessels, using computational fluid dynamic (CFD) simulation and the electrospinning technique, in order to recreate the natural environment for supporting EC survival and growth, hence the likelihood of long-term graft patency.

#### **Methods:**

**Materials:** Poly (vinyl alcohol) (PVA, 99% hydrolyzed, number average MW 89,000–98,000 g/mol) were obtained from Aldrich Chemical Co (UK). Gelatin (Ge) Type A (Approx. 300 Bloom) from porcine skin were obtained in powder form (Aldrich Chemical Co., UK). Methanol (99% Pure, HPLC grade), glacial acetic acid (99% pure) were obtained from Fisher scientific; Human Coronary Artery Endothelial Cells (HCAEC), passage 4 (PromoCell, Germany). Physiological Salt Solution (PSS) was prepared as previously described.<sup>33</sup>

**Scaffold design and fabrication:** Using computational fluid dynamic (CFD) simulation, a new scaffold structure with a small diameter of 4mm was designed with inner helices to enable a



'spiral flow' effect with better shear stress profile. The new scaffold model is a rigid tube with specific number of (2, 3 or 4) helices on the inner surface with different number of revolutions (1, 2 or 3) along the entire length (taken as 100mm). A starting angle of  $65^{\circ}$  for helix creation was used to eliminate any mismatch during anastomosis and obtain the best possible WSS distribution. To simplify the CFD analysis, blood flow was considered to be Laminar, and the unsteady three-dimensional Navier-Stokes equations were used as the governing rules. Blood was considered as homogeneous, incompressible, and Newtonian, with a constant viscosity of  $3.5 \times 10^{-3} \text{ kg}\cdot\text{m}^{-1}\cdot\text{s}^{-1}$  and density of  $1050 \text{ kg}\cdot\text{m}^{-3}$ . Reynolds number (Re) was kept at 300, as used in previous studies.<sup>34, 35</sup> The boundary conditions for the helical scaffold were then set as follow: (1) At the inlet, uniform velocity profile with a mean velocity of 0.372 m/s; (2) At the outlet, pressure, p was set at  $1.33 \times 10^4 \text{ Pa}$  (100 mmHg); (3) The vessel wall was assumed to be rigid and non-slippery. Simulation studies were then carried out and parameters such as shear stress and vorticity, in the centre and peripheral areas, were calculated and compared with the conventional scaffold as well as within the different helical scaffolds. Optimum designs were then selected for further consideration.

Small diameter vascular scaffolds were produced by electrospinning using a blend of PVA and gelatine (PVA:Ge 8:2). The scaffold design which displayed the best hemodynamic properties without affecting or obstructing the blood flow, was selected for further analysis. As part of this effort, a unique design with 2 helices and 1 pitch of rotation throughout scaffold length with starting angle of  $65^{\circ}$  was selected. This design creates swirling flow of the blood which was shown to perform best. To produce the conventional scaffold, a plain stainless-steel mandrel was used as a collector. It was imperative to optimise the rotating speed of the mandrel as being one of the process parameters that may affect the quality of the

fibrous structure. Therefore, the nanofibers were collected at rotating speeds of 1000 rpm when evaluated in terms of their morphological appearances and changes in alignments. The same size tubular mandrel with two helical grooves with one revolution and 1 mm depth was used as a collecting device to manufacture the helical scaffolds. Further information on manufacturing procedure for the helical scaffold design is detailed in a filed patent application No: GB1616064.

Electrospinning parameters used were as follows: Solution:- PVA M.Wt. 89,000–98,000 gm/mol; Gelatine Type A (300 Bloom); PVA solution 12.5% w/v in deionised water; Gelatine 12.5% w/v in Acetic acid:water ratio, 2:8; PVA: Ge mixing ratio, 8:2. Process parameters were: Voltage: 16 kV; Tip to collector distance: 15 cm; Flow rate: 1 ml/hr; Needle gauge: 18 G; Mandrel Diameter: 4 mm; Rotating speed: 1000 rpm. All the processes were carried out at room temperature and normal atmospheric humidity.

PVA and gelatine were dissolved in their corresponding solvents and the solutions were mixed together in a specific ratio of 8:2. The spinneret was traversing along the axis of the mandrel throughout its length to ensure uniform distribution of the fibre along the mandrel. Finished scaffolds (4 cm long) were allowed to dry overnight to ensure evaporation of residual solvents. In order to overcome instability in water, the scaffolds were cross-linked by physical (rather than chemical) means using methanol treatment. Methanol links the polymer network by intermolecular forces, including hydrogen bonding, and supports cell seeding and growth.<sup>28</sup> Fourier Transform Infra-Red spectroscopy (FTIR) analysis, differential scanning calorimetry (DSC), as well as dissolvability tests were carried out to identify any changes to the fibres after cross-linking (See supplementary information for details).

Scaffolds were subsequently stored in a sterile container for further mechanical and structural evaluation.

**Scaffold characterisation:** The *morphological characteristics* of the scaffolds were analysed by scanning electron microscopy (SEM; Hitachi, S3400N, Berkshire, UK). Scaffold and nanofibre samples were placed on aluminium stubs and sputter coated with gold/palladium for 45 sec at 18 mA using a sputter coater (Polaron Sc7620, Quorum technologies Ltd, UK), then scanned at an accelerating voltage of 7 kV. SEM images were captured to determine the inner and outer morphologies of the scaffolds and to evaluate the dimensions of the helices on the inner surface. Fibre diameter was measured by taking the average of 60 measurements chosen randomly from across the image, using Image J software (Image J, National Institutes of Health, Bethesda, USA). *Scaffold thickness* measurements were made using a high precision calliper. Five samples were measured per scaffold. The *tensile properties* of the electrospun fibrous membranes were determined using a universal tensile testing machine (INSTRON 2530). A test window frame was used to hold the membrane and measure its thickness using a micrometre screw gauge. The test specimen was then mounted on the tensile tester (specimen dimension: 50 x 12 mm; gauge length 24 mm; strain rate 5 mm/min; load cell 100 N). Only test samples that failed at least 2 mm from the edge of the tab were included in the test results for the calculation of the stress strain behaviour. For tensile testing of the tubular scaffolds, a 10 cm length was soaked in PSS overnight at room temperature, then mounting on a uniaxial load test machine equipped with a maximum 2kN load cell (cross head speed 0.5 mm/s). Tensile stress-strain plots were generated and the elastic modulus calculated using least-squares fit in the linear range of

the stress-strain plot. Ultimate tensile strength was measured as the highest stress value attained during the test. For *burst pressure testing*, an angioplasty balloon of matched diameter was inserted into the scaffold and hydrostatic pressure recorded until bursting occurred. The burst pressure was recorded as the maximum pressure prior to construct failure (n=5). In all cases, rupture occurred away from the cannulation site. To measure *suture retention strength*, the force necessary to pull a suture through the wall of electrospun scaffolds was measured. Three sutures were inserted 2 mm from the end of the scaffold at 90° angles and mounted on a tensile test instrument. One end of the scaffold was directly placed under the grips, while the other end was secured and pulled at a rate of 50 mm/min until the suture pulled through the vessel wall. *Compliance testing*: Scaffolds were mounted on cannulas using sutures and submerged in PSS (37°C). After equilibration, scaffolds were inflated from 0 to 200 mmHg in 10 mmHg increments using a syringe pump, then deflated again in 10 mmHg decrements. Outer diameters were recorded at each pressure level. Percentage diameter change relative to the diameter at 0 mmHg was calculated as  $\Delta D = (D_p - D_0) / D_0 \times 100$ ; where  $\Delta D$  is the percentage diameter change,  $D_p$  is the diameter at a specified pressure, and  $D_0$  is the reference diameter at 0 mmHg.

**Cell culture:** Human Coronary Artery Endothelial Cells (HCAEC) were grown as a monolayer at 37°C under 5% CO<sub>2</sub> atmosphere in EC growth medium MV (PromoCell) supplemented with 5% FCS (Invitrogen), 0.004 µl/ml endothelial growth supplement, 10 ng/ml epidermal growth factor and 90 µg/mL heparin. Cells were washed x3 in PBS and incubated with 0.1% trypsin for 3 min to detach them from the flask surface. Cells were then centrifuged at 220g for 3 min and resuspended in medium. Scaffolds were sterilized by immersion in 70%, 50%, 25% ethanol, and sterilized PBS (cell culture grade) for 30 min, washed twice, then

conditioned in growth medium overnight. Cells were seeded in the center of the scaffolds (100,000 cells) and both ends sealed with sterile thread and placed in an incubator for 2 hrs initially at 37°C, 5% CO<sub>2</sub> under constant rotation, on a flow circuit in culture medium. At specified time points (day 1, 3, and 5), seeded scaffolds were opened using a sterile razor along the length of the scaffold and analysed.

**Cell Morphology and distribution:** The morphology and proliferation of ECs seeded on the inner lumen of the scaffolds were examined by Scanning Electron Microscopy (SEM) and fluorescence microscopy. Seeded scaffolds were washed in PBS x3, fixed in 2.5% glutaraldehyde and dehydrated with a series of graded ethanol solutions. The dried samples were coated with gold using a sputter coater and observed by SEM under an accelerating voltage of 3 kV. Cells were analyzed using live/dead cell viability assay (Live/dead Cell Viability Assay kit, Invitrogen). Samples were washed for 5 min in PBS and incubated in a solution of 2 µM Calcein AM (live) and 4 µM Ethidium homodimer-1 (dead) solution in PBS for 30 min. Samples were imaged with an Inverted Fluorescence microscope using a conventional fluorescein long pass filter.

Distribution of ECs along the length of the scaffolds over 1-5 days (plus an extended time period of 7 days) was evaluated by monitoring cell metabolic activity at different locations within the scaffolds, using Presto Blue (PB) ( $n = 5$ ). Three samples (10x10 mm<sup>2</sup>) were taken from 3 different locations along the scaffold (one from the center and two 1.5 cm away from the site of seeding in both directions toward scaffold opening)<sup>33</sup>. PB reagent (1mL of 10%) was added to each well of a 24-well culture plate containing cell seeded scaffold, and incubated at 37 °C for 2 hrs. Changes in cell viability were detected using fluorescence read

at excitation 570 nm emission wavelength. Percentage reduction of PB was calculated according to supplier's information<sup>36</sup>.

**Measuring cell proliferation:** The degree of cell proliferation was measured indirectly through cell fluorescence methods as previously described<sup>37,38</sup> in the conventional and helical scaffolds, at days 1, 3, and 5. Total corrected cellular fluorescence was performed using Image J software, using the following formulas: total corrected cellular fluorescence (TCCF) = integrated density – (area of selected cell × mean fluorescence of background readings). Measurements of at least 5 cells were taken and averaged, for each scaffold.

**Pressure Myography studies:** Scaffolds were mounted on an inflow and outflow stainless steel cannulae within a pressure myography chamber and secured with ligatures. The cannula at the inflow site was connected to a pressure transducer and pressure servo control system (Living systems instrumentation, USA), and infused with PSS at 37°C. The chamber was placed under an inverted microscope, connected to a video dimension analyzer, camera and a monitor. The diameter of the scaffold was measured continuously using Lab Chart (AD instruments, UK). Both helical and conventional scaffolds were mounted before (day 0) and after complete endothelialization (at the extended time of 7 days). Intraluminal pressure was introduced via the pressure servo control system, at 60mmHg and 100 mmHg, over 1 hr. In another set of experiments, the scaffold's ability to withstand maximum pressure was assessed by increasing the pressure at 20 mmHg increments, up to the maximum retained in mmHg.

**Gene expression analysis:** HCAECs were seeded on the inner surface of the scaffold and allowed to proliferate over 4 days under static conditions to cover the entire surface of the

scaffold. Cell-seeded scaffolds (helical and conventional) were mounted on 4 mm stainless steel cannulas within a flow chamber and exposed to flow (Watson Marlow pump, UK) at 27  $\mu\text{l}/\text{min}$  for 0, 2, 6 and 24 hrs. Cells were then detached from the scaffold using TripleE and treated with RNA lysis buffer, snap frozen in dry ice, then stored at  $-80^{\circ}\text{C}$  for subsequent gene expression analysis, using the quantitative real-time polymerase chain reaction (qRT-PCR). Shear stress imparted on the endothelial cells was calculated using the following equation:

$$\tau = 4 \eta Q / \pi r^3$$

where  $\tau$  is shear stress ( $\text{dyn}/\text{cm}^2$ ),  $\eta$  is viscosity ( $0.007 \text{ dyn.s}/\text{cm}^2$ ),  $Q$  is flow (in  $\text{ml}/\text{s}$ ) and  $r$  is radius (in  $\text{cm}$ ).<sup>33</sup>

To analyse gene expression, RNA was isolated according to manufacturer protocol using GenElute Mammalian Total RNA Miniprep Kit (Sigma Aldrich, UK). The purity and concentration of RNA was measured using Nanodrop. The RNA was synthesized to cDNA using Random primer (250ng, Promega), dNTPs (0.5mM, Promega), 25U Superscript II (Invitrogen), RNase Out (Invitrogen), 0.1M DTT (Invitrogen) and 5x 1<sup>st</sup> strand buffer (Invitrogen). The level of gene expression was quantitatively determined using SensiMix SYBR<sup>®</sup> Low-ROX kit (Bioline). All PCR reactions were performed in biological and technical triplicates using Quant Studio 12K Flex instrument (Applied Biosystem). Each of the genes were normalized to housekeeping gene GAPDH and the relative gene expression were analysed using  $2^{-\Delta\Delta\text{CT}}$  method. Raw CT values greater than 35 were removed from analysis. Expression values were calculated using the formula:

$$E_x = 2^{(CT_{hk} - CT_x)}$$

Where  $CT_{hk}$  is the CT value of the housekeeping genes. P-values were calculated using Welch's t-test. All primers were designed using NCBI primer blast tool<sup>39</sup> and experimentally validated to have >98% efficiency with single dissociation peak. All the primer sequences are listed in Table 1.

**Statistical analysis:** All experiments were performed in quadruplicate at least three independent times, and the results presented are representative data sets. Cell counts are expressed as means  $\pm$ SD. Statistical analysis was performed using Student's t-test, where  $p < 0.05$  was considered significant.

## Results

**Hemodynamic analysis:** A comparison of haemodynamics performance between the various proposed designs was initially carried out. A considerable difference in WSS profile between the conventional and helical scaffolds was evident, when blood flow was simulated (Figure 1A). The observed WSS was much higher in scaffolds with 2 or 3 helices as compared to those with 1 helix feature or in the conventional scaffold. The insertion of more than 3 helices was excluded as this would result in higher resistance to flow, lower velocity of fluid and pressure drop which can lead to premature failure of the grafts.

**Fabrication and characterization of nano-fibrous scaffolds:** We developed a unique post-production technique to fabricate scaffolds with inner helices throughout their length



[Figure 1B]. The mechanical properties of the helical scaffold were comparable to that of human vessels, achieving similar ranges of wall thickness, compliance and elasticity to arteries<sup>40</sup> [Table 2]. Fibre diameter ranged from 320 nm to 520 nm in the scaffolds [Figure 1C]. The nanofibres observed on the luminal surface of the helical scaffold were randomly oriented and fine-structured resembling that of the ECM [Figure 1D].

***Cell viability, survival and distribution within the vascular scaffold:***

*Cell viability:* For both conventional and helical scaffolds, ECs adhered and spread very well on the surface of the scaffold over the 5 day incubation period [Figure 2A]. The Live–dead cell viability analysis on the luminal surface of the scaffolds revealed primarily live cells, with little evidence of dead cells. The green stained (live cells) and red stained (dead cells) ECs attached to the electrospun fibres of both scaffolds [Figure 2B]. Cells on the helical scaffold had a more elongated morphology and were more evenly distributed than cells grown on the conventional scaffold. ECs proliferated along the entire scaffold surface and by day 5, percentage live cells were  $94\% \pm 9\%$  and  $82\% \pm 7.2\%$  on the helical and conventional scaffolds, respectively. On the day of seeding, cells were present only in the center portion of the scaffold. As incubation time proceeded, a clear difference was observed in viable cell number and migration towards the peripheral area, between the helical and conventional scaffolds (Figure 2C). After 7 days, number of viable cells in the conventional grafts were  $4.64 \times 10^5 \pm 28,000$  cells/cm<sup>2</sup> (middle of the graft) and  $3.1 \times 10^5 \pm 15,000$  cells/cm<sup>2</sup> (near scaffold end). For helical scaffolds, there were  $5.2 \times 10^5 \pm 42,000$  cells/cm<sup>2</sup> (middle of the scaffold) and  $5.2 \times 10^5 \pm 36,000$  cells/cm<sup>2</sup> (near scaffold end) [ $p < 0.05$ ]. Hence, there was a

significant difference in cell distribution between helical and conventional scaffolds along its length. Also, migration was more uniform along the length of the helical than the conventional scaffold. These results are in line with the live dead cell viability analysis. In both cases, the growth rate for the first day after seeding was comparatively lower than the remaining incubation periods.

*Cell proliferation:* As a surrogate measure of cell proliferation, the degree of cell fluorescence was measured for cells in the conventional and helical scaffolds over the incubation periods, at days 1, 3, and 5. Total corrected cellular fluorescence was reduced over day 3 and 5 compared to day 1, for cells grown within the conventional scaffolds. In comparison, fluorescence levels were increased by over 10 fold after days 3 and 5 compared to day 1, for cells grown within the helical scaffolds (Figure 2D).

*Functional pressure analysis:* As a measure of improved surface coverage by ECs, the ability of endothelialized grafts to with-hold intraluminal pressure was evaluated by mounting the scaffolds within the pressure myography system. In the absence of any cells, scaffolds were not able to maintain intravascular pressure beyond 30 mmHg, over any length of time. After 7 days of culture both helical and conventional scaffolds were mounted onto the pressure chamber. Intravascular pressure was increased by 10 mmHg increments to 200 mmHg over a 1-hour time period. The maximum pressure achieved was 60 and 200 mmHg for conventional and helical scaffolds, respectively before starting to lose pressure (Figure 3A). In the next set of experiments, intravascular pressure was elevated to 60 mmHg and pressure retention monitored for both scaffolds. Within 45 min, the conventional scaffold started losing pressure, while the helical scaffold was able to sustain elevated pressure beyond 1 hr (Figure 3B).

*Cell adhesion and attachment during flow:* Cell adhesion was implicated by examining gene expression for adhesion molecules, in both types of scaffolds, at the early time points, under static conditions, initially. Significant elevation in CDH5 gene expression was evident at the early time points (2 and 6 hrs) in ECs from helical vs conventional scaffolds ( $p < 0.05$  and  $p < 0.01$  at 2 and 6 hr, respectively)- Figure 4A. Significant elevations were also evident after 6 hr for Beta 1 integrin ( $p < 0.05$ ), alpha 5 integrins ( $p < 0.01$ ), and VCAM-1 ( $p < 0.01$ ) in the helical scaffolds (versus conventional). These findings suggest that ECs grown within helical scaffolds show improved adhesion, over those grown within conventional scaffolds.

In order to recreate the physiological responses expressed by ECs, both conventional and helical scaffolds were seeded by ECs and maintained under flow conditions over 24 hrs (at  $0.5-1 \text{ dyn/cm}^2$ ). The influence of flow on gene expression was assessed at both the early (2, 6 hrs) and the longer time point of 24 hrs. At the early time points, elevation in adhesion molecule expression was evident in ECs from helical scaffolds for CDH5 (significant at 2 hr,  $p < 0.01$ ); for beta 1 integrin; alpha 5 integrins (significant at 2 and 6 hr,  $p < 0.05$  and  $p < 0.01$ , respectively); and VCAM-1 ( $p < 0.05$  and  $p = 0.05$ , at 2 and 6 hr respectively). For all adhesion molecules examined, there was no significant difference in expression between helical and conventional scaffolds, after 24 hrs. These results demonstrate that while improved adhesion was evident at the early time points within helical scaffolds, response to flow after 24 hrs was similar for ECs seeded in both conventional and helical scaffolds.

*Expression of mechanosensitive genes by ECs within scaffolds:* In the absence of flow, no overall mRNA expression of Nrf2 or HO.1 was evident in the conventional grafts at any of the time points. In the helical scaffolds, Nrf2 mRNA gene expression was significantly downregulated at 2 and 6 hr ( $p < 0.05$ ), but upregulated for HO.1 mRNA levels (significantly

at 6 hr,  $p < 0.01$ ). When flow was introduced, there was no overall increase in Nrf2 mRNA gene expression at any of the time points (2, 6, 24 hr), however, levels were clearly elevated for HO.1 mRNA levels (significant at 2hr and 24 hrs,  $p < 0.01$ ), in helical scaffolds. Exposure to flow over 24 hrs also led to a significant increase in KLF2 gene expression ( $p < 0.01$ ) [Figure 4 B]. Additionally, for Piezo 1, an important flow sensitive mediator of mechanotransduction, there was no upregulation in mRNA levels in the conventional scaffold under either the static or flow conditions. When flow was introduced, there was a significant upregulation in levels after 2 ( $p < 0.001$ ), 6 ( $p < 0.05$ ), and 24 hrs ( $p < 0.001$ ) in the helical scaffolds. ECs grown under flow conditions were thus flow responsive, especially when grown within helical scaffolds.

## Discussion

Using CFD simulation and the electrospinning technique, we have designed and fabricated a novel small diameter helical vascular scaffold that provides an improved niche for the survival of ECs, than conventional scaffolds, with improved responsiveness to shear stress and the ability to retain physiological levels of intravascular pressure.

A new design, which can provide spiral flow throughout the scaffold, was evaluated in the present study and parameters optimised to ensure that the generated spiral flow would be within the allowable physiological limits, as excessive amounts of WSS or blood particle velocity can damage the vessel walls and produce adverse effects.<sup>41</sup> CFD experiments related to spiral geometries have previously mainly focused on physical twisting of the principal geometry.<sup>42, 43</sup> Shorter helical pitch or larger amplitude are known to enhance

WSS in 3D geometries and decrease the low and high velocity zone ratios.<sup>29, 30</sup> It has been established that normalised axial WSS would potentially improve mass transfer and minimum pressure drop on graft with internal helices angles in the region of 40° to 65°. Although such designs have had beneficial effects, they can increase pressure drop, which can lead to excessive flow resistance at fixed flow rates which may create haemodynamic failure.<sup>42</sup> Also, the flow profile can cause flow stagnation and inhabitation which makes the graft vulnerable to intimal hyperplasia and thrombosis, if implanted.<sup>42</sup> Furthermore, due to the twisting effect, change in the physical geometry is relatively sharp, which could lead to sudden alteration in shear stress levels and have adverse effects on the cells. Therefore, an optimal structural design was required which would provide a gradual change in the spiral geometry thus providing better validation with the natural flow profile and uniform WSS distribution. Hence, the proposition to insert helices within the inner walls rather than the physical twisting of the whole graft was adopted in the present study. Using numerical simulation, Kabinejadian and colleagues were able to demonstrate significant effectiveness of out-of-plane helicity and spiral ridge features of grafts in inducing swirling flow. This was influenced by ridge height and number of ridges where multi-ridge designs result in higher WSS magnitudes on the arterial bed, further confirming our findings.<sup>44</sup> Our helical scaffolds were fabricated using the electrospinning technology. Using electrospinning in conventional form, other researchers have been able to produced 3D nano-fibrous tubular scaffolds with a large range of vessel diameters.<sup>24</sup> The morphological and mechanical analysis performed on our electrospun scaffolds confirmed the presence of the helical structure within the tubular scaffold with mechanical properties comparable to those of native vessels. Moreover, as the delivery needle was continuously travelling along the length of the mandrel, tubular structures of uniform thickness were produced.<sup>24</sup>

One of the major reasons attributed to graft failure is the lack of a uniform layer of ECs on the graft surface or poor attachment of the cells. ECs cultured within our helical scaffolds demonstrated improved viability and proliferation in comparison to those cultured within the conventional scaffolds, over the 5-7 day incubation period. Furthermore, there was a significant increase in cell distribution over the length of the helical than the conventional scaffolds. This was further confirmed by assessing the ability of the cell-seeded scaffolds to withstand physiological ranges of intravascular pressure. Our endothelialized helical scaffolds were better able to withstand and sustain physiological pressures within the range that vessels of similar diameter are exposed to *in vivo*. This may relate to improved cell attachment, distribution and spreading along the entire surface of the helical scaffold. Improved cell viability, proliferation and distribution, is supported by evidence of improved cell-cell contact and cell adhesion to the electrospun fibres, as shown by upregulated expression of CDH5, Beta 1 integrin, alpha 5 integrins, and VCAM-1, in the helical scaffolds.<sup>45, 46</sup>

Whilst integrin molecules are associated with mechanotransduction, other mechanosensitive genes are also key to the transmission of mechanical stimuli into intracellular biochemical signals. These include genes associated with atheroprotective responses, such as Nrf2. The latter is a key transcription factor that is highly sensitive to laminar shear stress, leading to its increased stability and its translocation to the nucleus where it binds to the anti-oxidant response element (ARE) of antioxidant genes, including heme oxygenase-1 (HO-1).<sup>19</sup> Gene upregulation was initially examined herein, in ECs grown in conventional and helical scaffolds under static conditions. EC seeded scaffolds were subsequently exposed to flow over a 24 hr period (at 0.5-1 dyn/cm<sup>2</sup>), in order to recreate the physiological responses *in vivo* and assess the responsiveness to acute effects of shear

stress on EC gene upregulation. Our results demonstrate that while improved adhesion was evident at the early time points within helical scaffolds, the response to flow after 24 hrs was similar for ECs seeded in both conventional and helical scaffolds. Nonetheless, the significant upregulation of the mechanosensitive genes (HO.1; Peizo1; KLF2) after 24hrs confirms EC responsiveness to the shear stress imparted by the fluid flow within the helical scaffolds. Whist Nrf2 gene expression was unaltered, we show a significant increase in HO.1 expression after flow, consistent with previous findings.<sup>19, 47</sup> The expression of adhesion molecules and mechanosensitive genes has previously been demonstrated within ECs exposed to steady laminar flow at a range of flow rates within 7 -24 hrs.<sup>21, 46, 48-50</sup> The significant increase in KLF2 gene expression demonstrated in the present study after exposure to flow (24 hr,  $p < 0.01$ ), further supports the increase in HO.1 expression since KLF2 has been shown to upregulate the expression of antioxidant pathways and also eNOS, hence generation of nitric oxide, supporting atheroprotection.<sup>19, 50</sup>

In conclusion, we have designed and fabricated a novel small diameter helical vascular scaffold that provides an improved niche for the survival of ECs, over a conventional tubular scaffold. The novel scaffold environment enables enhanced cell viability and distribution, and demonstrates improved responsiveness to shear stress and ability to retain physiological levels of intravascular pressure. Hence, in addition to showing potential as a graft for preclinical testing, these helical scaffolds can be utilised as a tool to study EC behaviour under an environment that mimics more closely the natural structure of real vessels.

**Acknowledgements**

This work was supported by a 'Joint health accelerator grant' from the University of Manchester and Manchester Metropolitan University (2015/16). We thank Dr Robert Lowe, Queen Mary Westfield University, UK, for cartoon illustrations.



## References:

1. Benjamin EJ, Blaha MJ, Chiuve SE, Cushman M, Das SR, Deo R, et al. Heart Disease and Stroke Statistics'2017 Update: A Report from the American Heart Association. *Circulation* 2017;**135**:e146–603. doi:10.1161/CIR.0000000000000485.
2. Pries AR, Badimon L, Bugiardini R, Camici PG, Dorobantu M, Duncker DJ, et al. Coronary vascular regulation, remodelling, and collateralization: Mechanisms and clinical implications on behalf of the working group on coronary pathophysiology and microcirculation. *Eur Heart J* 2015;**36**:3134–46. doi:10.1093/eurheartj/ehv100.
3. Mohr FW, Morice M-C, Kappetein AP, Feldman TE, Stähle E, Colombo A, et al. APPENDIX- Coronary artery bypass graft surgery versus percutaneous coronary intervention in patients with three-vessel disease and left main coronary disease: 5-year follow-up of the randomised, clinical SYNTAX trial. *Lancet* 2013;**381**:629–38. doi:10.1016/S0140-6736(13)60141-5.
4. Chlupac J, Filova E, Bacakova L, Chlupac J, Filová E, Bačáková L. Blood vessel replacement: 50 years of development and tissue engineering paradigms in vascular surgery. *Physiol Res* 2009;**58**:119–39. doi:931918 [pii].
5. Desai M, Seifalian AM, Hamilton G. Role of prosthetic conduits in coronary artery bypass grafting. *Eur J Cardio-Thoracic Surg* 2011;**40**:394–8. doi:10.1016/j.ejcts.2010.11.050.
6. Brien TO, Walsh M, McGloughlin T. On reducing abnormal hemodynamics in the femoral end-to-side anastomosis: The influence of mechanical factors. *Ann Biomed Eng* 2005;**33**:310–22. doi:10.1007/s10439-005-1733-y.

7. G N, Tan A, Gundogan B, Farhatnia Y, Nayyer L, Mahdibeiraghdar S, et al. Tissue engineering vascular grafts a fortiori: looking back and going forward. *Expert Opin Biol Ther* 2015;**15**:231–44. doi:10.1517/14712598.2015.980234.
8. Furchgott RF, Zawadzki J V. The obligatory role of endothelial cells in the relaxation of arterial smooth muscle by acetylcholine. *Nature* 1980;**288**:373–6. doi:10.1038/288373a0.
9. Vanhoutte PM, Shimokawa H, Tang EHC, Feletou M. Endothelial dysfunction and vascular disease. *Acta Physiol* 2009;**196**:193–222. doi:10.1111/j.1748-1716.2009.01964.x.
10. Walden R, L'italien GJ, Megerman J, Abbott WM. Matched Elastic Properties and Successful Arterial Grafting. *Arch Surg* 1980;**115**:1166–9. doi:10.1001/archsurg.1980.01380100018004.
11. Peiffer V, Sherwin SJ, Weinberg PD. Computation in the rabbit aorta of a new metric - the transverse wall shear stress - to quantify the multidirectional character of disturbed blood flow. *J Biomech* 2013;**46**:2651–8. doi:10.1016/j.jbiomech.2013.08.003.
12. Coppola G, Caro C. Arterial geometry, flow pattern, wall shear and mass transport: potential physiological significance. *J R Soc Interface* 2009;**6**:519–28. doi:10.1098/rsif.2008.0417.
13. Segadal L, Matre K. Blood velocity distribution in the human ascending aorta. *Circulation* 1987;**76**:90–100. doi:10.1161/01.CIR.76.1.90.
14. Caro CG, Watkins N, Doorly DJ, Sherwin SJ, Peiró J. Influence of non-planar geometry

- on flow separation. *J Physiol* 1998;**513**.
15. Lurie F, Kistner RL. On the existence of helical flow in veins of the lower extremities. *J Vasc Surg Venous Lymphat Disord* 2013;**1**:134–8. doi:10.1016/J.JVSV.2012.08.002.
  16. Stonebridge PA, Brophy CM. Spiral laminar flow in arteries? *Lancet* 1991;**338**:1360–1. doi:10.1016/0140-6736(91)92238-W.
  17. Chiu J-J, Chien S. Effects of disturbed flow on vascular endothelium : pathophysiological basis and clinical perspectives. *Physiol Rev* 2011;**91**:327–87. doi:10.1152/physrev.00047.2009.
  18. Xu S, Koroleva M, Yin M, Jin ZG. Atheroprotective laminar flow inhibits Hippo pathway effector YAP in endothelial cells. *Transl Res* 2016;**176**:18–28.e2. doi:10.1016/j.trsl.2016.05.003.
  19. McSweeney SR, Warabi E, Siow RCM. Nrf2 as an Endothelial Mechanosensitive Transcription Factor: Going With the Flow. *Hypertension* 2016;**67**:20–9. doi:10.1161/HYPERTENSIONAHA.115.06146.
  20. Balaguru UM, Sundaresan L, Manivannan J, Majunathan R, Mani K, Swaminathan A, et al. Disturbed flow mediated modulation of shear forces on endothelial plane: A proposed model for studying endothelium around atherosclerotic plaques. *Sci Rep* 2016;**6**. doi:10.1038/srep27304.
  21. Amaya R, Pierides A, Tarbell JM. The Interaction between Fluid Wall Shear Stress and Solid Circumferential Strain Affects Endothelial Gene Expression. *PLoS One* 2015;**10**:1–18. doi:10.1371/journal.pone.0129952.
  22. Okuhn SP, Connelly DP, Calakos N, Ferrell L, Man-Xiang P, Goldstone J. Does

- compliance mismatch alone cause neointimal hyperplasia? *J Vasc Surg* 1989;**9**:35–45.  
doi:10.1016/0741-5214(89)90217-6.
23. Liao R, Green NE, Chen SYJ, Messenger JC, Hansgen AR, Groves BM, et al. Three-dimensional analysis of in vivo coronary stent--coronary artery interactions. *Int J Cardiovasc Imaging* 2004;**20**:305–13.
24. Hasan A, Memic A, Annabi N, Hossain M, Paul A, Dokmeci MR, et al. Electrospun scaffolds for tissue engineering of vascular grafts. *Acta Biomater* 2014;**10**:11–25.  
doi:10.1016/j.actbio.2013.08.022.
25. Ahn H, Ju YM, Takahashi H, Williams DF, Yoo JJ, Lee SJ, et al. Engineered small diameter vascular grafts by combining cell sheet engineering and electrospinning technology. *Acta Biomater* 2015;**16**:14–22. doi:10.1016/j.actbio.2015.01.030.
26. Yu E, Zhang J, Thomson JA, Turng LS. Fabrication and characterization of electrospun thermoplastic polyurethane/fibroin small-diameter vascular grafts for vascular tissue engineering. *Int Polym Process* 2016;**31**:638–46. doi:10.3139/217.3247.
27. Teo WE, Kotaki M, Mo XM, Ramakrishna S. Porous tubular structures with controlled fibre orientation using a modified electrospinning method. *Nanotechnology* 2005;**16**:918–24. doi:10.1088/0957-4484/16/6/049.
28. Miraftab M, Saifullah AN. Physical stabilisation of electrospun poly (vinyl alcohol) nanofibres: comparative study on methanol and heat-based crosslinking. *J Mater Sci* 2015;  
**50**: 1943-1957.

29. Nuttelman CR, Mortisen DJ, Henry SM, Ameth KS. Attachment of fibronectin to poly(vinyl alcohol) hydrogels promotes NH3T3 cell adhesion, proliferation, and migration. *J. Biomed. Mater. Res* 2001; **2**:217-223.
30. Chu KC, and Rutt BK. Polyvinyl alcohol cryogel: An ideal phantom material for MR studies of arterial flow and elasticity. *Magn. Reson. Med.* 1997; **37**: 314-319.
31. Malafaya PB, Silva GA, Reis RL. Natural-origin polymers as carriers and scaffolds for biomolecules and cell delivery in tissue engineering applications. *Adv. Drug Deliv. Rev.* 2007; **59**: 207-233.
32. Atlan M, Simon-Yarza T, Ino JM, Hunsinger V, Corte L, Ou P, Ald-Launais R, Chaouat M, Letourneur D. Design, characterisation and in vivo performance of synthetic 2 mm-diameter vessel grafts made of PVA-gelatin blends. *Sci Reports* 2018; **8**: 7417-7435.
33. Azzawi M, Austin C. The effects of endothelial factor inhibition on the time course of responses of isolated rat coronary arteries to intraluminal flow. *J Vasc Res* 2007;**44**:223–33. doi:10.1159/000100421.
34. Oshima M, Torii R, Kobayashi T, Taniguchi N, Takagi K. Finite element simulation of blood flow in the cerebral artery. *Comput Methods Appl Mech Eng* 2001;**191**:661–71. doi:10.1016/S0045-7825(01)00307-3.
35. Benim AC, Nahavandi A, Assmann A, Schubert D, Feindt P, Suh SH. Simulation of blood flow in human aorta with emphasis on outlet boundary conditions. *Appl Math Model* 2011;**35**:3175–88. doi:10.1016/j.apm.2010.12.022.
36. Lall N, Henley-Smith CJ, De Canha MN, Oosthuizen CB, Berrington D. Viability reagent, prestoblue, in comparison with other available reagents, utilized in cytotoxicity and

- antimicrobial assays. *Int J Microbiol* 2013;**2013**. doi:10.1155/2013/420601.
37. Gavet O, Pines J. Activation of cyclin B1-Cdk1 synchronizes events in the nucleus and the cytoplasm at mitosis. *J Cell Biol* 2010;**189**:247–59. doi:10.1083/jcb.200909144.
38. McCloy RA, Rogers S, Caldon CE, Lorca T, Castro A, Burgess A. Partial inhibition of Cdk1 in G2phase overrides the SAC and decouples mitotic events. *Cell Cycle* 2014;**13**:1400–12. doi:10.4161/cc.28401.
39. <https://www.ncbi.nlm.nih.gov/tools/primer-blast/> last accessed March 2017.
40. Stekelenburg M, Rutten MCM, Snoeckx LHEH, Baaijens FPT. Dynamic Straining Combined with Fibrin Gel Cell Seeding Improves Strength of Tissue-Engineered Small-Diameter Vascular Grafts. *Tissue Eng Part A* 2009;**15**:1081–9. doi:10.1089/ten.tea.2008.0183.
41. Zhang JM, Zhong L, Su B, Wan M, Yap JS, Tham JPL, et al. Perspective on CFD studies of coronary artery disease lesions and hemodynamics: A review. *Int J Numer Method Biomed Eng* 2014;**30**:659–80. doi:10.1002/cnm.2625.
42. Sun A, Fan Y, Deng X. Numerical comparative study on the hemodynamic performance of a new helical graft with noncircular cross section and swirlGraft. *Artif Organs* 2010;**34**:22–7. doi:10.1111/j.1525-1594.2009.00797.x.
43. Cookson AN, Doorly DJ, Sherwin SJ. Mixing through stirring of steady flow in small amplitude helical tubes. *Ann Biomed Eng* 2009;**37**:710–21. doi:10.1007/s10439-009-9636-y.
44. Kabinejadian F, McElroy M, Ruiz-Soler A, Leo HL, Slevin MA, Badimon L, et al. Numerical assessment of novel helical/spiral grafts with improved hemodynamics for

- distal graft anastomoses. *PLoS One* 2016;**11**. doi:10.1371/journal.pone.0165892.
45. Sun X, Fu Y, Gu M, Zhang L, Li D, Li H, et al. Activation of integrin  $\alpha 5$  mediated by flow requires its translocation to membrane lipid rafts in vascular endothelial cells. *Proc Natl Acad Sci* 2016;**113**:769–74. doi:10.1073/pnas.1524523113.
46. Lu X, Kassab GS. Integrins mediate mechanical compression–induced endothelium-dependent vasodilation through endothelial nitric oxide pathway. *J Gen Physiol* 2015;**146**:221–32. doi:10.1085/jgp.201411350.
47. Warabi E, Takabe W, Minami T, Inoue K, Itoh K, Yamamoto M, et al. Shear stress stabilizes NF-E2-related factor 2 and induces antioxidant genes in endothelial cells: Role of reactive oxygen/nitrogen species. *Free Radic Biol Med* 2007;**42**:260–9. doi:10.1016/j.freeradbiomed.2006.10.043.
48. Björck HM, Renner J, Maleki S, Nilsson SFE, Kihlberg J, Folkersen L, et al. Characterization of Shear-Sensitive Genes in the Normal Rat Aorta Identifies Hand2 as a Major Flow-Responsive Transcription Factor. *PLoS One* 2012;**7**. doi:10.1371/journal.pone.0052227.
49. Dekker RJ, Van Soest S, Fontijn RD, Salamanca S, De Groot PG, VanBavel E, et al. Prolonged fluid shear stress induces a distinct set of endothelial cell genes, most specifically lung Krüppel-like factor (KLF2). *Blood* 2002;**100**:1689–98. doi:10.1182/blood-2002-01-0046.
50. Parmar KM, Larman HB, Dai G, Zhang Y, Wang ET, Moorthy SN, et al. Integration of flow-dependent endothelial phenotypes by Kruppel-like factor 2. *J Clin Invest* 2006;**116**:49–58. doi:10.1172/JCI24787.

**TABLE LEGENDS**

**Table 1:** List of Primers used for qRT-PCR to assess gene expression patterns by endothelial cells.

**Table 2:** Comparative mechanical properties of electrospun helical grafts (4 mm internal diameter) with that of human vessels.

**FIGURE LEGENDS**

**Figure 1:** Scaffold fabrication and characterisation. (A) Scanning electron micrograph of the conventional and helical scaffolds showing the inside structure with inner helices identified for the helical scaffold. (B) The wall shear stress profile of the conventional and helical scaffolds with a number of helices on the inner surface. A histogram showing fibre diameter range (C) and distribution (D) of the fabricated scaffolds.

**Figure 2:** Endothelial cell culture and distribution within the conventional and helical scaffolds. (A) Scanning electron micrographs of Human Coronary Artery Endothelial Cells (HCAEC) cultured on the inner side of conventional and helical electrospun scaffolds (3 keV). (B) Live–dead cell staining of endothelial cells seeded on conventional and helical scaffolds. Assay stains are merged [live cells green, dead cells red (nuclei only)]. Figures are representative of the scaffold. Scale bar is 25 $\mu$ m. (C) Cell viability across the entire scaffold,



assessed using the Presto Blue assay. The results are expressed as means ( $\pm$ ) SD. \* $p < 0.05$ .

(D) Degree of cell fluorescence of the HCAECs after seeding in the conventional and helical scaffolds. \*\*  $p < 0.001$ .

**Figure 3:** Pressure retention within the helical and conventional grafts after a 7 day incubation period with ECs. A) Maximum intraluminal pressure achieved after step-wise elevation in pressure. B) Intraluminal pressure monitoring over a period of 1 hour after pressure elevation to 60 mmHg. \* $p < 0.01$ ;  $n = 5$ .

**Figure 4:** Adhesion molecule and mechanosensitive gene expression by endothelial cells (ECs) seeded within the conventional and helical scaffolds, over acute times of 2, 6, and 24hr, in the absence and presence of flow. (A) significant elevation in adhesion molecule expression for beta 1 integrin, alpha 5 integrin and VCAM-1 is evident in the helical scaffolds, under static and early time points of flow. (B) Flow induced a significant elevation in HO.1 but not Nrf-2 mRNA in the helical scaffolds. Flow also induced a significant elevation in KLF2 and Piezo-1 mRNA expression by ECs from the helical scaffolds in comparison to those from conventional scaffolds.

**Table 1: List of Primers used for qRT-PCR.**

GENE	SPECIES		SEQUENCE
VE-Cadherin	Human	FWD	CTTCACCCAGACCAAGTACACA
		REV	GGCTCATGTATCGGAGGTCG
VCAM-1	Human	FWD	GTTTGCAGCTTCTCAAGCTTTTA
		REV	TCACCTTCCCATTCAAGTGA
Integrin $\alpha$ 5	Human	FWD	CCAGATCCTGTCTGCCACTC
		REV	GTAGGAGGCCATCTGTTCCC
Integrin $\beta$ 1	Human	FWD	CCGCGCGGAAAAGATGAAT
		REV	ATGCATCTGGAGGGCAACC
NRF2	Human	FWD	GTGCTGTCAAGGGACATGGA
		REV	TTTGGGAATGTGGGCAACCT
HO-1	Human	FWD	GACAGCATGCCCCAGGATTT
		REV	ATCACCAGCTTGAAGCCGTC
KLF2	Human	FWD	CGGCAAGACTACACCAAGA
		REV	TGGTAGGGCTTCTCACCTGT
Piezo1 (FAM38A)	Human	FWD	GCTGAAAAGACAGATGGAGCG
		REV	CCTCGGGTCTTCAGGAACAG
GAPDH	Human	FWD	AGGCTTTGGACGCCTCTGGAA
		REV	CGAATGACACCGTACTCCTCATAGAAGCT

**TABLE 2:** Comparative mechanical properties of electrospun helical grafts (4 mm internal diameter) with that of human vessels (from published literature).<sup>40</sup>

Sample		Wall Thickness ( $\mu\text{m}$ )	Burst Pressure (mm Hg)	% Compliance (100 mm Hg)	Suture retention (g)	Young's Modulus ( $\text{N/m}^2$ )
Electrospun <i>helical Scaffold</i>		$350 \pm 20$ (n=10)	$1010 \pm 200$ (n=5)	$3.2 \pm 0.4$ (n=20)	$162 \pm 15$ (n=5)	$1.8 \times 10^8$
Native tissue	<i>Saphenous vein</i>	110-550	1600	0.7-1.5	$196 \pm 2$	/
	<i>Artery</i>	350-700	2000	4.5-6.2	$200 \pm 120$	$1.2 - 1.3 \times 10^5$

Graphical abstract text- Parikh *et al.*

We used an intelligent design system and the electrospinning technique to synthesise 'small' diameter nanofibrous helical scaffolds with inner ridges to allow spiral flow. Human endothelial cells survived well on the inner scaffold layer with better ability to withhold elevated intravascular pressures, than conventional scaffolds. Our novel helical scaffold can be explored as a potential small diameter graft to treat cardiovascular disease patients.

ACCEPTED MANUSCRIPT

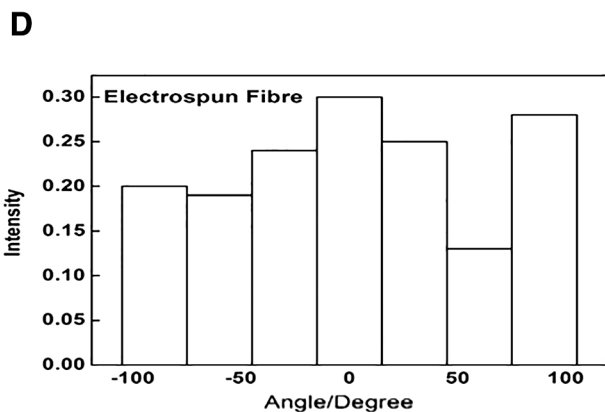
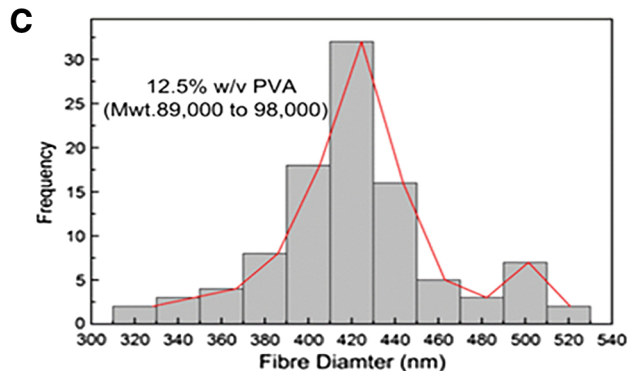
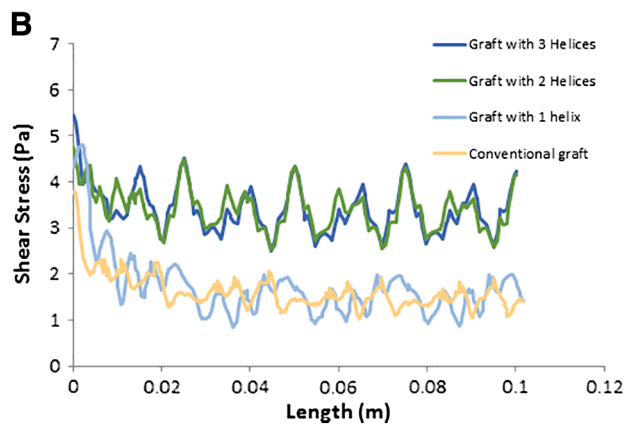
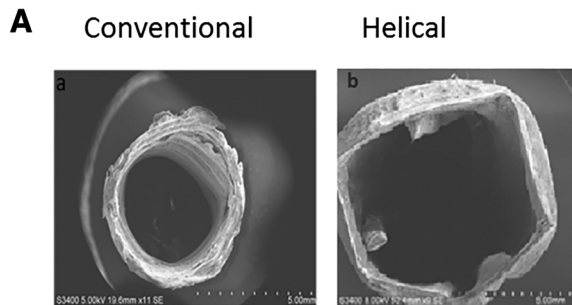


Figure 1

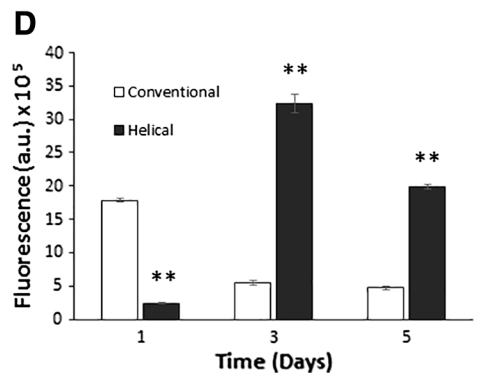
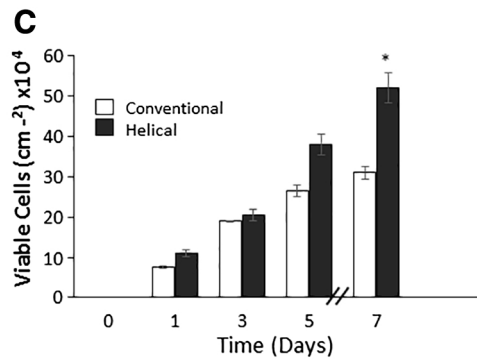
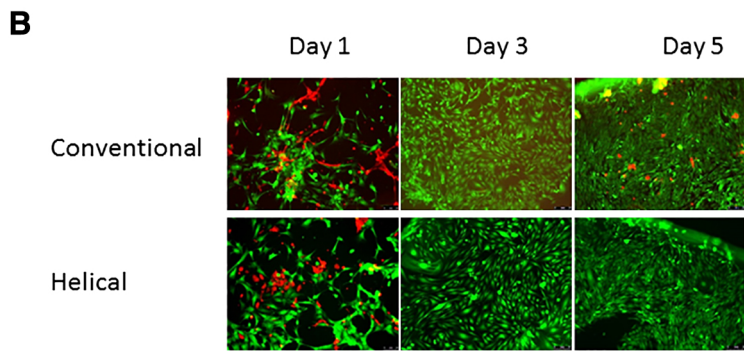
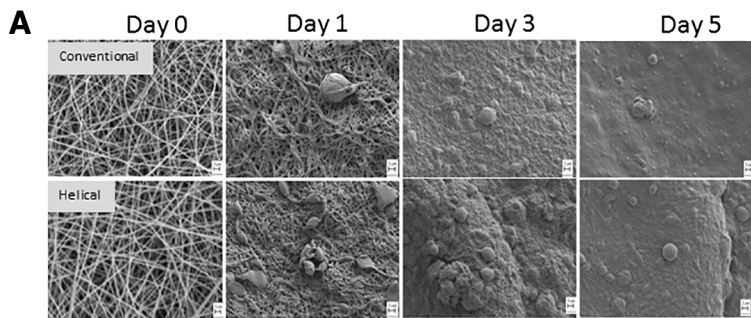


Figure 2

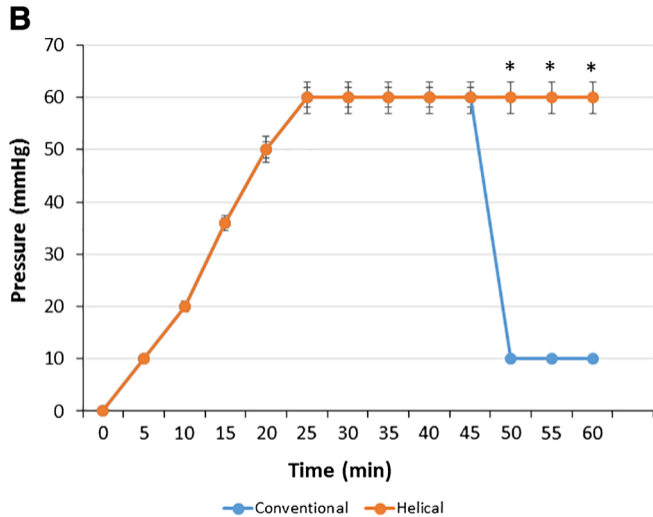
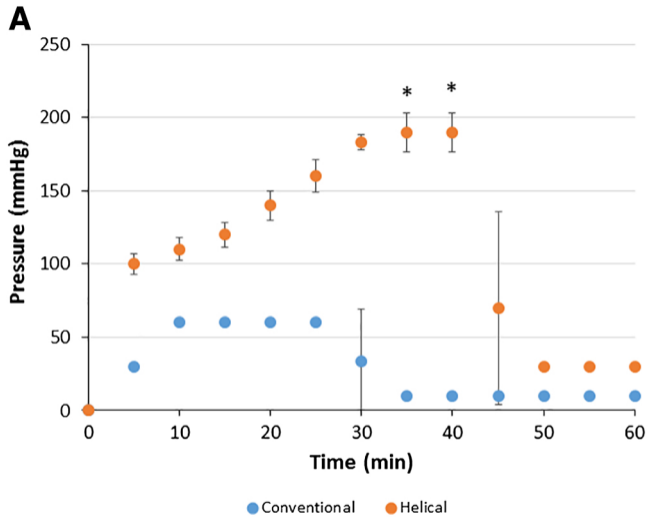


Figure 3

A

0H

2H

6H

24H

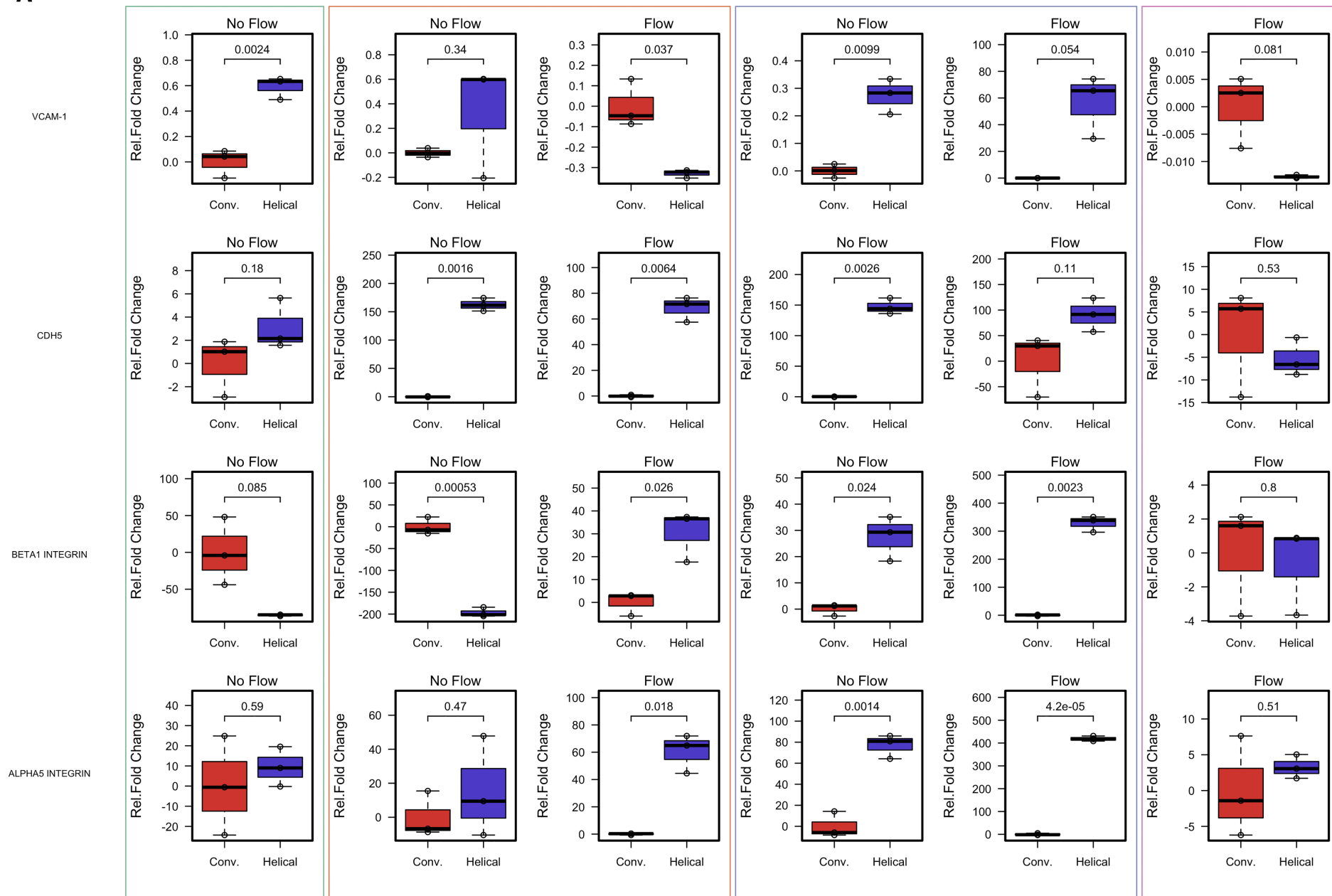


Figure 4a



**B**

0H

2H

6H

24H

HO.1

NRF2

Piezo-1

KLF2

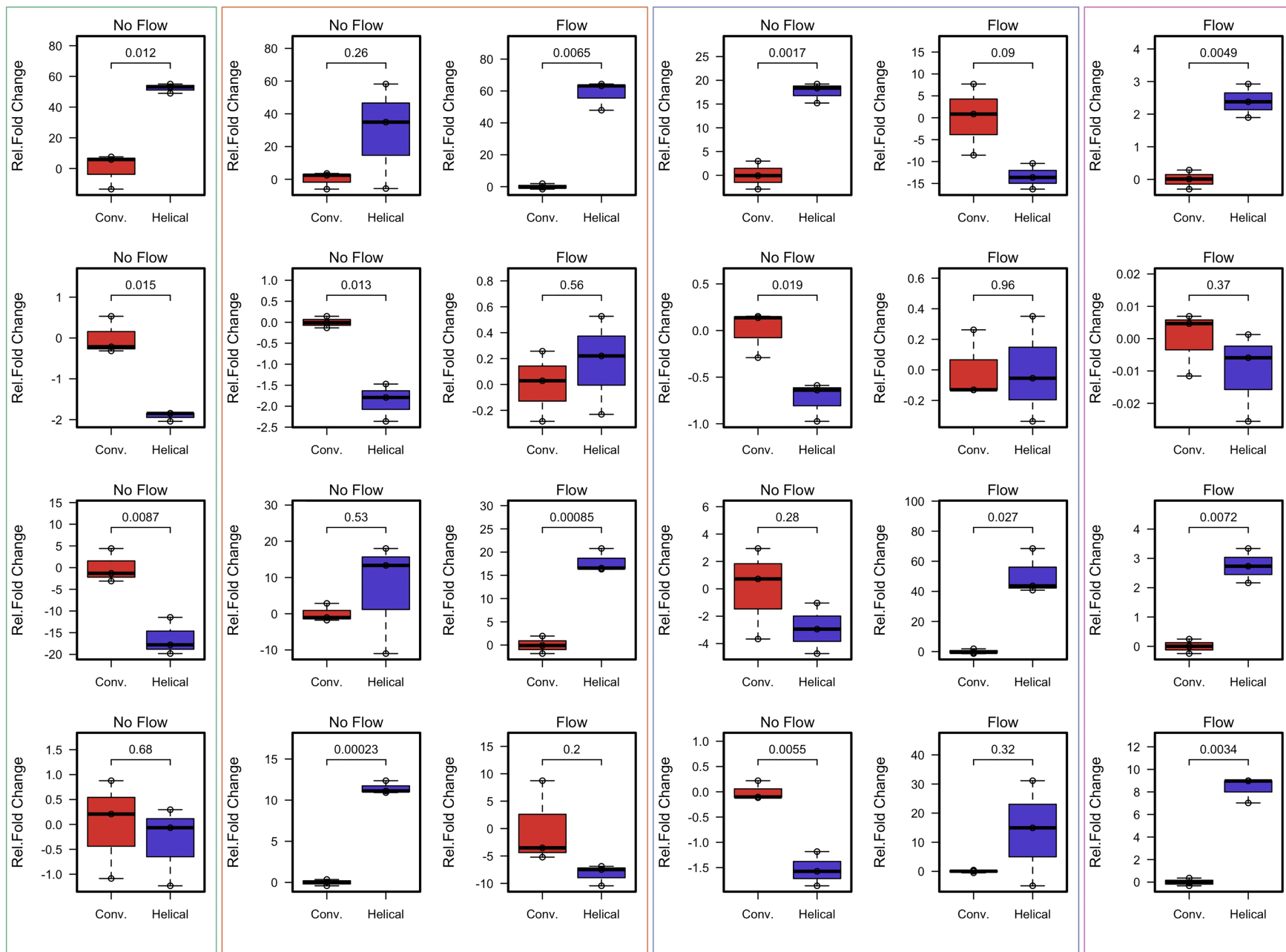


Figure 4b